

# MYB30 links ROS signaling, root cell elongation, and plant immune responses

Kaho Mabuchi<sup>a</sup>, Hiromasa Maki<sup>a</sup>, Tomotaka Itaya<sup>b</sup>, Takamasa Suzuki<sup>b,c,d</sup>, Mika Nomoto<sup>b</sup>, Satomi Sakaoka<sup>e,f,g</sup>, Atsushi Morikami<sup>g</sup>, Tetsuya Higashiyama<sup>b,d,h</sup>, Yasuomi Tada<sup>b,e</sup>, Wolfgang Busch<sup>i</sup>, and Hironaka Tsukagoshi<sup>e,f,g,1</sup>

<sup>a</sup>Graduate School of Bioagricultural Science, Nagoya University, Nagoya, 464-8602 Aichi, Japan; <sup>b</sup>Division of Biological Science, Graduate School of Science, Nagoya University, Nagoya, 464-8602 Aichi, Japan; <sup>c</sup>Department of Biological Chemistry, College of Bioscience and Biotechnology, Chubu University, Kasugai, 478-8501 Aichi, Japan; <sup>d</sup>Exploratory Research for Advanced Technology Higashiyama Live-Holonics Project, Nagoya University, Nagoya, 464-8602 Aichi, Japan; <sup>e</sup>The Center for Gene Research, Nagoya University, Nagoya, 464-8602 Aichi, Japan; <sup>f</sup>Precursory Research for Embryonic Science and Technology, Japan Science and Technology Agency, Kawaguchi, 332-0022 Saitama, Japan; <sup>g</sup>Faculty of Agriculture, Meijo University, Nagoya, 468-8502 Aichi, Japan; <sup>h</sup>Institute of Transformative Bio-Molecules, Nagoya University, Nagoya, 464-8602 Aichi, Japan; and <sup>i</sup>Plant Molecular and Cellular Biology Laboratory, Salk Institute for Biological Studies, La Jolla, CA 92037

Edited by Natasha V. Raikhel, Center for Plant Cell Biology, University of California, Riverside, CA, and approved April 6, 2018 (received for review March 15, 2018)

Reactive oxygen species (ROS) are known to be important signal molecules that are involved in biotic and abiotic stress responses as well as in growth regulation. However, the molecular mechanisms by which ROS act as a growth regulator, as well as how ROS-dependent growth regulation relates to its roles in stress responses, are not well understood. We performed a time-course microarray analysis of *Arabidopsis* root tips upon treatment with hydrogen peroxide, which we named “ROS-map.” Using the ROS-map, we identified an MYB transcription factor, MYB30, which showed a strong response to ROS treatment and is the key regulator of a gene network that leads to the hydrogen peroxide-dependent inhibition of root cell elongation. Intriguingly, this network contained multiple genes involved in very-long-chain fatty acid (VLCFA) transport. Finally, we showed that *MYB30* is necessary for root growth regulation during defense responses, thus providing a molecular link between these two ROS-associated processes.

ROS | transcriptional regulation | root development | lipid transfer | plant immune response

Roots anchor the plant and acquire water and nutrients from the soil. For water and nutrient acquisition, the root's ability to sense changes in the surrounding environment and adjust its growth in response to these external stimuli is critical. These growth responses depend primarily on the balance between cellular proliferation and differentiation in the root tip. Using the root of the model species *Arabidopsis thaliana*, multiple molecular mechanisms for regulating the balance of proliferation and differentiation have been identified. The best-described mechanism is the cross-talk among plant hormones, which act as signal molecules that control root development by regulating transcriptional networks (1). More recently, reactive oxygen species (ROS) have been identified as important signal molecules that regulate root development and specifically the balance between cell proliferation and differentiation (2, 3). Interestingly, ROS are also implicated in a multitude of other processes ranging from cell wall synthesis (4) to plant defense (5). A major question is whether and how these diverse functions of ROS are interconnected.

UP BEAT1 (UPB1), a basic helix-loop-helix (bHLH) type transcription factor, has been shown to be one of the key players in the developmental function of ROS. Several peroxidases, which are direct targets of UPB1, control the balance of two different types of ROS, superoxide and hydrogen peroxide (H<sub>2</sub>O<sub>2</sub>), and consequently the balance of cell proliferation and differentiation (6). The molecular role of H<sub>2</sub>O<sub>2</sub> in the regulation of cell proliferation has been demonstrated to be due to the repression of cell-cycle-related genes in the meristematic zone of the root (7).

While these developmental functions of ROS have emerged rather recently, the involvement of ROS in stress responses has

been known for a long time (8). Under many abiotic stress conditions, such as salinity, drought, UV, and high light, cellular ROS levels increase (9). This increase seems to be tightly regulated. An example is salt stress in which genes involved in ROS metabolism are up-regulated in a specific tissue-type and time-dependent manner (10).

ROS production in the root is also induced by biotic stress. In fact, very high rates of ROS production (oxidative burst) are observed as one of the earliest responses to pathogens (11). The burst leads to toxicity toward invading pathogens as well as to cell-wall modifications that are thought to fortify the cell wall (12). It is elicited by microbe-associated molecular patterns (MAMPs) such as Flg22 (13). Much like many abiotic stresses, Flg22 treatment is accompanied by both an increase in ROS levels and cessation of root growth (14). Taken together, this suggests that the ROS signaling network tunes plant growth to biotic and abiotic stress conditions. However, the molecular basis of this integration is unknown.

Here, we used a transcriptome approach that we designated “ROS-map” to identify genes that respond to ROS in a

## Significance

Plant roots tune their growth to the environment. An important class of molecules involved in environmental responses as well as in root growth regulation is composed of reactive oxygen species (ROS). By making use of a comprehensive transcriptome atlas capturing ROS responses in different developmental zones of the root, we uncovered a regulatory network that is involved in root-growth regulation and responses to biotic stress. This network is composed of the ROS-responsive transcription factor MYB30, which regulates multiple genes involved in the transport of very-long-chain fatty acids (VLCFAs). Overall, our findings show that *Arabidopsis* uses the same MYB30-dependent regulatory network for root-growth and immunity responses, processes that were considered largely independent of each other.

Author contributions: K.M., Y.T., and H.T. designed experiments; K.M., H.M., T.I., T.S., M.N., S.S., and H.T. performed experiments; K.M., T.S., A.M., T.H., W.B., and H.T. analyzed experiments; and W.B. and H.T. wrote the paper.

The authors declare no conflict of interest.

This article is a PNAS Direct Submission.

Published under the PNAS license.

Data deposition: The microarray dataset has been deposited at the National Center for Biotechnology Information Gene Expression Omnibus (GEO) database (accession number GSE85015). All RNA-seq files have been deposited at the DNA Data Bank of Japan database as series record DRA005125.

<sup>1</sup>To whom correspondence should be addressed. Email: thiro@meijo-u.ac.jp.

This article contains supporting information online at [www.pnas.org/lookup/suppl/doi:10.1073/pnas.1804233115/-DCSupplemental](http://www.pnas.org/lookup/suppl/doi:10.1073/pnas.1804233115/-DCSupplemental).

Published online April 30, 2018.

developmental zone-specific manner. Using this ROS-map, we identified MYB30 as a key transcription factor that orchestrates ROS-dependent developmental responses resulting in cellular elongation in the root. A part of this developmental response is mediated by genes that are involved in the transport of very-long-chain fatty acids (VLCFAs). Interestingly, MYB30, as well as some of its target genes, functions not only in ROS-dependent developmental processes but also in defense responses toward bacterial elicitors. Overall, our findings show that *Arabidopsis* uses the same MYB30-dependent regulatory network for root growth and immunity, processes which previously have been thought to be largely independent of each other.

## Results

### Transcriptional Response to ROS Is Dynamic and Developmental Zone Specific

Although there is much evidence that ROS are important signaling molecules in root development, not much is known about the molecular mechanism underlying ROS-dependent regulation. To identify genes that regulate root development in a H<sub>2</sub>O<sub>2</sub>-dependent manner, we performed a time-course microarray analysis of roots treated with H<sub>2</sub>O<sub>2</sub> for 1, 3, or 6 h. To assess expression responses of proliferating and elongating cells, we harvested the meristematic and elongation zones separately. Based on these experiments, we identified 201 genes that were specifically up-regulated in the meristematic zone and 265 genes that were up-regulated only in the elongation zone in at least one time point (Fig. 1A). Eighty-three genes were up-regulated in both zones, and 25 genes were down-regulated in both zones. One hundred ninety genes were down-regulated only in the meristematic zone, and 192 genes were down-regulated only in the elongation zone.

We next investigated whether genes involved in specific biological processes were enriched in these gene sets. Gene ontology (GO) enrichment analysis revealed multiple processes that are targeted by the genes that are differentially expressed upon H<sub>2</sub>O<sub>2</sub> treatment in a developmental zone-specific manner (Fig. 1B and C). After 6 h treatment, GO categories involved in stress responses such as heat, cold, and UV were enriched for the up-regulated genes. A notable GO category enrichment among down-regulated genes in the meristematic zone was cell wall modification (Fig. 1D). In the elongation zone, GO categories related to salicylic acid (SA) and jasmonic acid (JA) responses were found to be enriched for genes that were up-regulated within 1 and 3 h after H<sub>2</sub>O<sub>2</sub> treatment. After 6 h of treatment, the lipid-transport and lipid-binding categories were detected as enriched in the up-regulated genes, while five GO categories were detected as enriched among the down-regulated genes in the elongation zone (Fig. 1E). Overall, these results indicate that there is a distinct spatial and temporal transcriptional pattern in response to H<sub>2</sub>O<sub>2</sub>.

### MYB30 Regulates Cellular Expansion in the Root in Response to ROS.

Transcription factors are key players in orchestrating stress and developmental responses. We therefore analyzed the ROS-map for differentially expressed transcription factors. We found 50 up-regulated transcription factors (Fig. 1F). Reassuringly, among these were multiple transcription factors implicated in ROS signaling-dependent stress responses such as *ZAT12* (15), *ZAT10* (16), and *DREB2A* (17). Since MYB30 (At3g28910) showed the most prominent H<sub>2</sub>O<sub>2</sub> response among the up-regulated transcription factors and was induced by H<sub>2</sub>O<sub>2</sub> in both the meristematic and elongation zones, we hypothesized that MYB30 is downstream of ROS signaling and regulates root development.

To test this hypothesis, we first reconfirmed by RT-qPCR that MYB30 expression is induced by H<sub>2</sub>O<sub>2</sub> in the whole root (Fig. S1A). We then characterized the phenotype of two transfer DNA (T-DNA) insertion lines, *myb30-1* and *myb30-2* (Fig. S1B), both of which had greatly reduced levels of MYB30 (Fig. S1C). We assessed root-growth rates for these lines when treated with 500-μM H<sub>2</sub>O<sub>2</sub> for 24 h (Fig. S1D). On Murashiga and Skoog

(MS, i.e. control) medium, the root-growth rates were not significantly different from wild-type plants. On H<sub>2</sub>O<sub>2</sub> medium, however, the root-growth rate of the two mutant lines was significantly higher than that of wild-type plants. For our subsequent mutant analysis, we focused on the *myb30-2* mutant line to avoid potentially confounding results from the *myb30-1* line, which has an additional insertion in the *THA2* (At3g04520) ORF resulting in the down-regulation of *THA2* expression (Fig. S1E).

To obtain a more detailed view of the role of MYB30, we performed time-lapse imaging to determine root-elongation rates upon H<sub>2</sub>O<sub>2</sub> treatment (Fig. 2A and Movie S1). The growth dynamics were similar for mutant and wild-type plants under control conditions. Strikingly, the elongation rate of *myb30-2* increased to a higher degree than that of wild-type plants after 400 min, resulting in a 400-μm-longer root (Col-0: 1,027 μm ± 257 μm; *myb30-2*: 1,433 μm ± 285 μm) after 20 h of treatment. These results suggest that MYB30 dynamically regulates root growth in response to H<sub>2</sub>O<sub>2</sub>.

To investigate the *myb30-2* phenotype at the cellular level (Fig. 2B), we measured cortical cell numbers in the meristematic zone, the length of the meristematic zone, cortical cell numbers in the elongation zone, the length of the elongation zone, and the length of the last cortical cell of the elongation zone under control and 500-μM H<sub>2</sub>O<sub>2</sub> treatments (Fig. 2C and Fig. S1F and G). Cortical cell numbers in the meristematic and the elongation zones and length of the meristematic zone were not statistically different between wild-type and *myb30-2* plants in both control and H<sub>2</sub>O<sub>2</sub> treatments. By contrast, the length of the elongation zone and the length of the last cortical cell of the elongation zone were increased in the *myb30-2* mutant compared with wild-type plants specifically under H<sub>2</sub>O<sub>2</sub> treatment. These results show that MYB30 regulates root cell elongation in response to H<sub>2</sub>O<sub>2</sub>.

Using the 35S promoter, we generated a MYB30 overexpressor (MYB30-OX) line in the *myb30-1* background. As we had fused YFP to the N terminus of MYB30 cDNA, we could visually confirm widespread the expression of the 35S:YFP-MYB30 construct, and we also checked MYB30 expression levels in MYB30-OX lines by RT-qPCR (Fig. S2A and B). The root length of MYB30-OX lines was significantly shorter than that of wild-type plants even under control conditions (Fig. S2C and D). While we later discovered the additional insertion in the *THA2* locus in the *myb30-1* line, this opposite phenotype to both *myb30* lines suggested that this shorter-root-length phenotype is due solely to the overexpression of MYB30.

To further test this in the *myb30-2* background, we constructed an estradiol-inducible version of MYB30 by cloning the YFP-MYB30 gene into *pMDC7* (18) and transformed this construct into *myb30-2*. We first investigated induction levels of MYB30 after 1, 3, 6, and 24 h of 5-μM estradiol treatment (Fig. S2E). MYB30 expression was strongly induced after 1 h of estradiol treatment in the induction line. By using this induction line, we performed time-lapse imaging and measured root elongation every 20 min (Fig. 2D and Movie S2). Root elongation of Columbia-0 (Col-0) (wild-type) and *pXVE-YFP-MYB30/myb30-2* plants was almost the same until 280 min after estradiol treatment. Moreover, we measured relative YFP intensity from YFP-MYB30 (Fig. 2E), which showed a rapid increase after 80 min of estradiol treatment. These data demonstrate that MYB30 is sufficient to inhibit root elongation. Taken together, our data indicate that MYB30 regulates root growth in response to ROS at the level of cellular elongation.

**MYB30 Is Expressed in the Root Tip in a ROS-Dependent Manner.** To illuminate the spatiotemporal aspects of the MYB30 response to H<sub>2</sub>O<sub>2</sub> in the root, we observed MYB30 transcriptional (*pMYB30:GFP*) and translational (*pMYB30:YFP-MYB30*) fusions. While there was almost no detectable fluorescent signal in root tips of both fusions in standard conditions (Fig. S3A and B), a weak signal could be detected in the epidermis of the meristematic zone of the *pMYB30:GFP* line after 1 h of H<sub>2</sub>O<sub>2</sub> treatment. After 24 h of treatment, the transcript was stronger and was detected

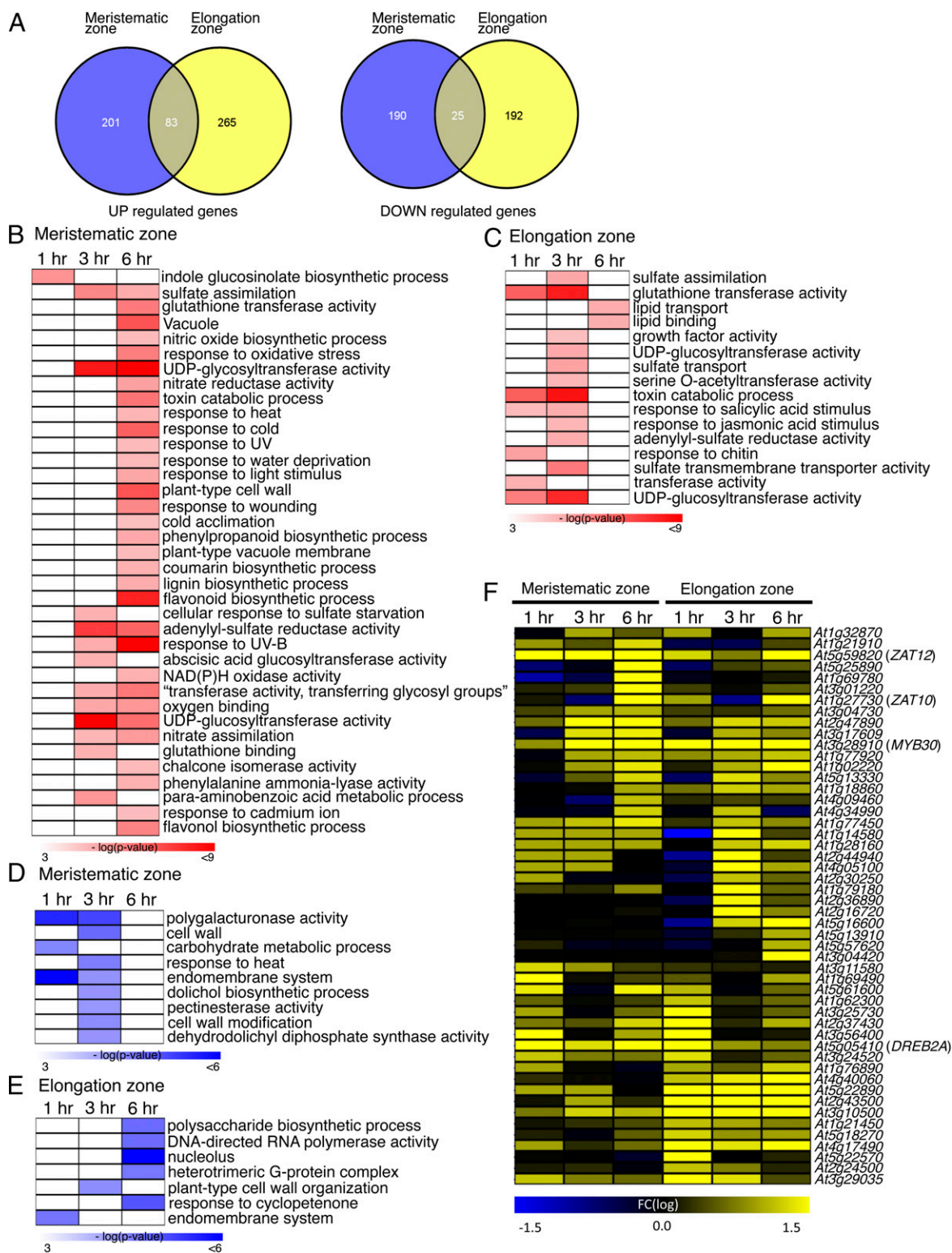


**Fig. 1.** ROS-map: Transcriptome analysis of ROS-responsive genes in different zones of the *Arabidopsis* root tip. (A) Venn diagrams of the significantly responding genes (twofold change, FDR < 0.05) in the meristematic (blue) and elongation (yellow) zones in at least one time point in the time-course microarray. (B–E) Enriched GO categories for tissues over time. (B and C) GO categories enriched among genes significantly up-regulated upon  $H_2O_2$  treatment in the meristematic zone (B) and elongation zone (C). (D and E) GO categories enriched among genes significantly down-regulated upon  $H_2O_2$  treatment in the meristematic zone (D) and elongation zone (E). (F) Heat map of 50 transcription factor genes that exhibited significantly induced gene expression upon  $H_2O_2$  treatment in at least one time point. Rows: genes; columns: samples; color: FC compared with T0 (see key).

throughout the epidermal and cortical cell files in the meristematic and elongation zones (Fig. S3A). Concomitantly, 24 h of  $H_2O_2$  treatment of the *pMYB30:YFP-MYB30* lines resulted in the

accumulation of YFP-MYB30 in the epidermis and cortex as well as in the vasculature in the maturation zone (Fig. S3B). Moreover, the *pMYB30:YFP-MYB30* lines complemented the



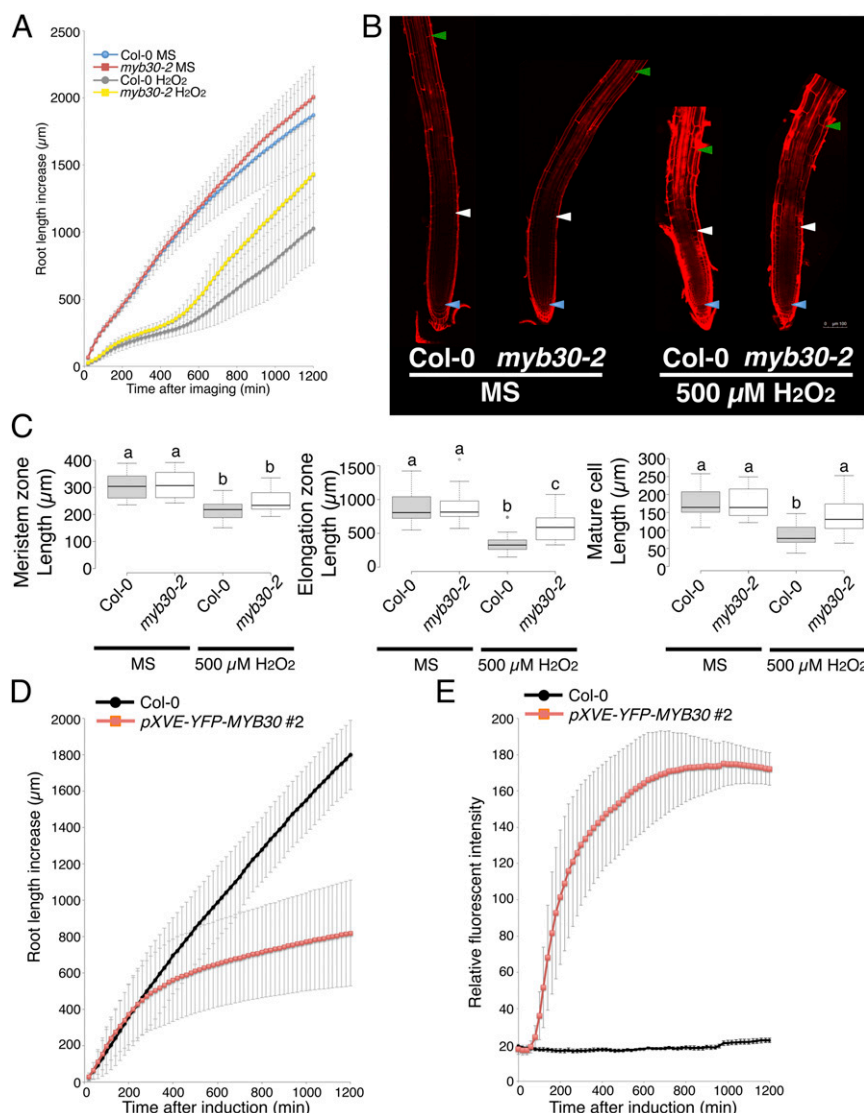


**Fig. 2.** Root phenotypes of *myb30* mutants and *MYB30* estradiol-induction lines. (A) Root length increase in Col-0 and *myb30-2* plants treated with control MS or with 500-μM H<sub>2</sub>O<sub>2</sub>. The root length increase was measured every 20 min after the starting point by time-lapse imaging ( $n = 5$ , respectively,  $\pm$ SD). (B) Confocal microscope images of 5-dai Col-0 and *myb30-2* plants treated with control MS or with 500-μM H<sub>2</sub>O<sub>2</sub> for 1 d. The quiescent center cells (blue arrowheads), the end of the meristematic zone (white arrowheads), and the end of the elongation zone (green arrowheads) are indicated. (Scale bars, 100 μm.) (C) Box plots for lengths of the meristematic zone, the elongation zone, and mature cells of Col-0 (gray boxes) and *myb30-2* (white boxes) plants treated with control MS or 500-μM H<sub>2</sub>O<sub>2</sub> for 1 d ( $n = 12$ ). Letters above the boxes indicate statistically significant differences between samples as determined by Tukey's honestly significant difference (HSD) test ( $P < 0.01$ ). (D) The increase in the length in 5-dai roots of Col-0 (black circles) and *pXVE::YFP-MYB30/myb30-2* (red squares) plants treated with 5-μM estradiol. Root length increase was measured every 20 min after the starting time by time-lapse imaging ( $n = 7$ , respectively,  $\pm$ SD). (E) Quantification of relative YFP fluorescence intensity of Col-0 (black circles) and *pXVE::YFP-MYB30/myb30-2* (red squares) plants treated with 5-μM estradiol ( $n = 7$ , respectively,  $\pm$ SD).

root-length phenotype of *myb30-2* after H<sub>2</sub>O<sub>2</sub> treatment (Fig. S3 C and D). Interestingly, restoration of the root growth to wild-type levels, as opposed to the growth suppression that we observed in the ectopic overexpression (Fig. S2D), occurred regardless of the *MYB30* base-level expression in the complementation lines, suggesting that overexpression in the native expression domain does not interfere with *MYB30* function.

Consistent with the microarray data, *MYB30* is induced within 60 min after H<sub>2</sub>O<sub>2</sub> treatment in the meristematic and elongation zones of the root. However, *MYB30* is not expressed in all tissues but is expressed mainly in the epidermal and cortical cell layers of the root tip. This suggests that the early effect on root growth is exerted largely in the epidermal and cortex layers.

**MYB30 Regulates Specific Sets of Genes.** To identify genes downstream of *MYB30* whose expression is regulated in the presence of H<sub>2</sub>O<sub>2</sub>, we selected genes differentially expressed among Col-0,

*myb30-2*, and *MYB30-OX* plants that either were not treated or were treated with 500-mM H<sub>2</sub>O<sub>2</sub> for 24 h using RNA-sequencing (RNA-seq). Under control conditions, three genes were significantly down-regulated and one gene was up-regulated in *myb30-2* plants. After H<sub>2</sub>O<sub>2</sub> treatment, nine genes were down-regulated and one gene was up-regulated in *myb30-2* plants (Fig. S4). We then compared Col-0 with *MYB30-OX* and identified 203 genes that were up-regulated and 548 genes that were down-regulated in the control condition (Dataset S1). Four hundred seventy-three genes were up-regulated and 110 genes were down-regulated in *MYB30-OX* upon H<sub>2</sub>O<sub>2</sub> treatment (Dataset S1). Among the nine genes that showed significant expression changes in *myb30-2* plants treated with H<sub>2</sub>O<sub>2</sub>, we found six genes that were also upregulated in the *MYB30-OX* datasets: lipid transfer protein 5 (*LTP5*, *At3g51600*), GPI-anchored lipid transfer protein 1 and 2 (*LTPG1*, *At1g27950*, and *LTPG2*, *At3g43720*, respectively), pectin methylesterase 44 (*PME44*, *At4g33220*), glycine-rich protein 5

(GRP5, *At3g20470*), and aldehyde dehydrogenase 3F1 (*At4g36250*). The expression of these six genes was also induced upon H<sub>2</sub>O<sub>2</sub> treatment in Col-0 plants (Fig. S4). We then identified MYB30 coexpression clusters based on large sets of published transcriptome data using ATTED II (19). Five of these six genes were represented in this coexpression dataset (Fig. S5A), suggesting that they are regulated by MYB30. In our ROS-map dataset (Fig. S5B) we saw that MYB30 was induced 1 h after H<sub>2</sub>O<sub>2</sub> treatment, and *LTP5*, *LTPG1*, *LTPG2*, and *PME44* were induced 3 h after H<sub>2</sub>O<sub>2</sub> treatment. The transcripts of the remaining gene, *GRP5*, were detected only at a very low level in the ROS-map, which led us to exclude it from further analysis. The temporal delay in gene expression of *LTP5*, *LTPG1*, *LTPG2*, and *PME44* is consistent with their being downstream of MYB30 in response to H<sub>2</sub>O<sub>2</sub>. Moreover, according to the Root Map datasets (20), these genes are expressed in the same root cell types as MYB30 (Fig. S5C). Furthermore, we independently confirmed by RT-qPCR that expression of these genes was strongly reduced in *myb30-2* plants and was up-regulated in *MYB30-OX* plants (Fig. 3A). The wild-type-like gene-expression response to H<sub>2</sub>O<sub>2</sub> was restored in *myb30-2* lines complemented with YFP-MYB30 driven by the endogenous MYB30 promoter (Fig. S5D), showing that the transcriptional regulation of these genes is MYB30 dependent.

We further investigated the expression levels of these putative MYB30 target genes using MYB30 estradiol induction lines treated for 1, 3, 6, or 24 h with estradiol (Fig. 3B). The four putative target genes showed no induction after 1-h treatment. However, there was strong induction after 3-h treatment. This

time delay between MYB30 and its candidate target genes was again suggestive of a transcriptional cascade.

Interestingly, this putative downstream gene cluster is related to lipid metabolism and signaling. To test whether this was a general pattern, we analyzed GO categories of genes differentially expressed in Col-0 and MYB30-OX plants (Fig. S5 E–G). Indeed, GO categories that were up-regulated in MYB30-OX plants included VLCFA metabolic process, lipid transport, and lipid binding. GO categories that were up-regulated in MYB30-OX plants upon H<sub>2</sub>O<sub>2</sub> treatment also included VLCFA metabolic process, lipid transport, lipid binding, and suberin biosynthetic process. These results are consistent with the ROS-map result that showed that lipid transport and lipid binding in the elongation zone were enriched after 6-h H<sub>2</sub>O<sub>2</sub> treatment and point toward an important role for these processes in ROS-dependent root-growth control.

**MYB30 Directly Binds to the Promoter Region of *LTP5*, *LTPG1*, and *LTPG2*.** To determine if these genes are direct targets of MYB30, we used ChIP of the YFP-MYB30 protein from the MYB30-OX line and subsequent qPCR detection of promoter fragments (ChIP-qPCR). Previous studies had indicated that GTTTGTT is the MYB30 *cis*-element (21). However, we could not find a perfect MYB30 *cis*-element within the promoter regions of *LTP5*, *LTPG1*, and *PME44*. We found a GTTTGTA element in the *LTP5* promoter (base pairs –656 to –650), GTTTGTT in the *LTPG1* promoter (base pairs –908 to –902), and multiple GTTGTTT elements in the *PME44* promoter region

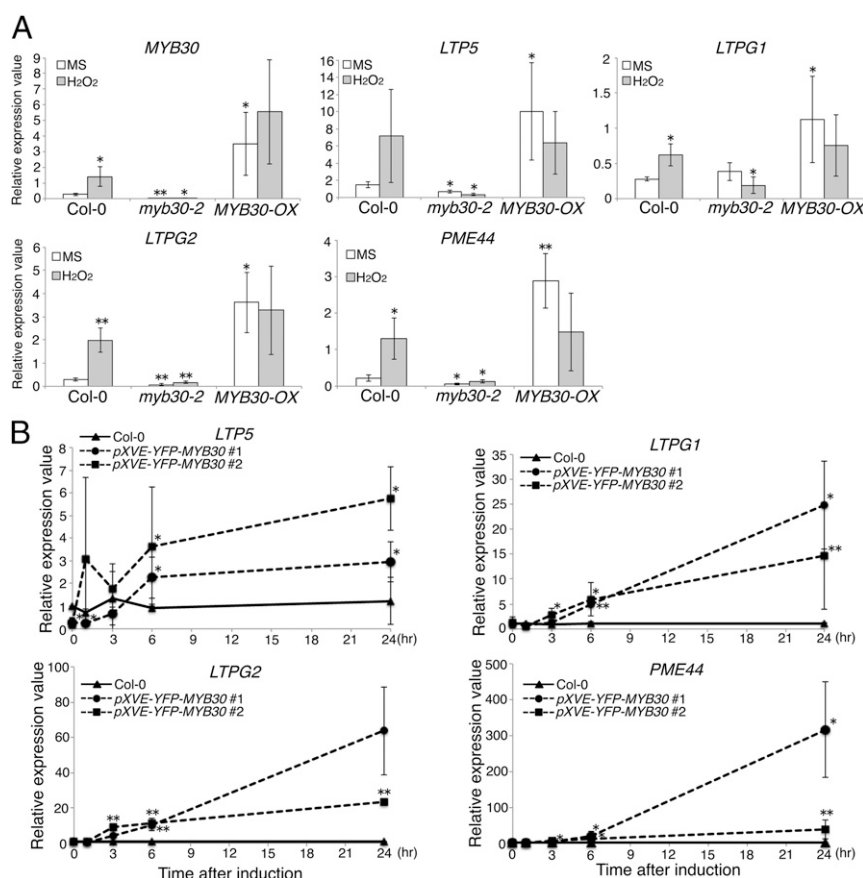


**Fig. 3.** Expression analysis of MYB30 target genes in the *myb30-2* and MYB30-OX lines. (A) RT-qPCR analysis of MYB30 and its putative target genes in the root tip of Col-0, *myb30-2*, and MYB30-OX line #1 plants ( $n = 3$ ;  $\pm$ SD). White bars: MS control; gray bars: 500- $\mu$ M H<sub>2</sub>O<sub>2</sub> treatment for 1 d. \*\* $P < 0.01$  and \* $P < 0.05$  compared with Col-0 control treatment, Student's  $t$  test. (B) Time-course RT-qPCR analysis for the expression of MYB30 target genes after 0, 1, 3, 6, or 24 h of 5- $\mu$ M estradiol treatment in the root tip of Col-0 plants (triangle with solid lines) and two independent transgenic pXVE::YFP-MYB30/*myb30-2* lines (circles and squares with dashed lines) ( $n = 3$ ;  $\pm$ SD). \*\* $P < 0.01$  and \* $P < 0.05$  compared with Col-0 at each time point, Student's  $t$  test.

(base pairs -1,362 to -1,356, -1,061 to -1,053, -518 to -512, and +676 to +683). As for the *LTPG2* promoter, we found a GTTGTG motif at position -428 to -422. Based on these data we designed PCR primer sets for these motifs for the *LTP5*, *LTPG1*, *LTPG2*, and *PME44* promoter regions (denoted "primer set #2"), as well as primer sets for sequences around 500–1,000 bp upstream or downstream of these elements (denoted "primer set #1" and "primer set #3," respectively). We detected significant enrichment for the *LTP5*, *LTPG1*, and

*LTPG2* promoter regions (Fig. 4A) as well as MYB30 binding to the *PME44* #2 and #3 regions in which at least four MYB30 potential binding elements are located. These results indicate that *LTP5*, *LTPG1*, *LTPG2*, and *PME44* are direct targets of MYB30.

It was striking that *LTP5* was regulated by MYB30 on the transcriptional level and that the ChIP suggested that MYB30 was binding directly to a noncanonical motif. We therefore set out to further test whether MYB30 could bind to the motifs present in

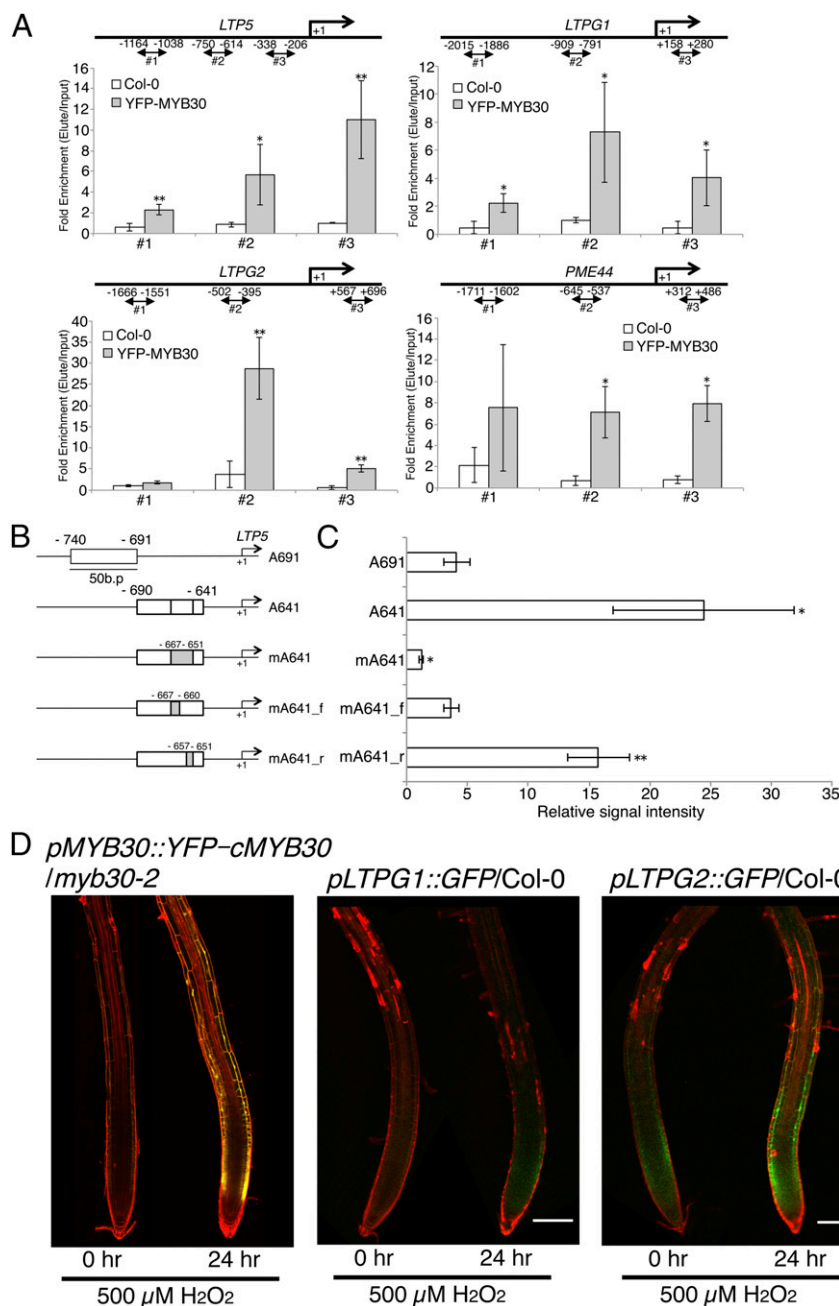


**Fig. 4.** DNA-binding analysis of MYB30 and expression patterns of MYB30 target genes. (A) ChIP-qPCR analysis of the in vivo binding assay for MYB30. Two-headed arrows below the each gene indicate the position of amplicons in this assay. White bars indicate the ChIP from Col-0 plants, and gray bars indicate the ChIP from *35S::YFP-MYB30* plants ( $n = 3$ ;  $\pm$ SD). \*\* $P < 0.01$  and \* $P < 0.05$  compared with each Col-0 signal, Student's  $t$  test. (B) Schematic representation of the structure of the probes used for the AlphaScreen. The numbers show the position of the *LTP5* upstream regions. White boxes indicate the probes, and gray boxes indicate the regions where mutations were introduced. (C) In vitro interaction of recombinant MYB30-FLAG with biotinylated DNA probes as evaluated by AlphaScreen ( $n = 3$ ;  $\pm$ SD). \*\* $P < 0.01$  and \* $P < 0.05$  compared with the signal of A691, Student's  $t$  test. (D) Expression of *pMYB30::YFP-MYB30* in the *myb30-2* background, *pLTPG1::GFP* in the Col-0 background, and *pLTPG2::GFP* in the Col-0 background. Plants were treated with 500- $\mu$ M H<sub>2</sub>O<sub>2</sub> for 0 or 24 h at 5-dai. Two confocal images were superimposed for aligning 0 hr 500  $\mu$ M H<sub>2</sub>O<sub>2</sub> with 24 hr 500  $\mu$ M H<sub>2</sub>O<sub>2</sub> treatments on the black background. (Scale bars, 100  $\mu$ m.)



the *LTP5* promoter. For this, we used the AlphaScreen assay. We produced a MYB30-FLAG tag fusion protein using an in vitro transcription-translation protein synthesis system (Fig. S6). As a target sequence, we used a MYB30-binding *cis*-element-like sequence, *GTTTGTGA* (indicated in italics) in the *LTP5* promoter at position –657 to –651 bp upstream of the start codon. Moreover, we noticed that the adjacent sequence contained an additional MYB30 *cis*-element-like sequence, *GTTGTTGTAGGTTTGTGA* (indicated by underlining). We thus designed five DNA probes for the AlphaScreen system (Fig. 4B): A641 (no mutations), mA641 (mutations introduced in all the *GTTGTTGTAGGTTTGTGA* region), mA641\_f (mutations introduced in the *GTTGTTGT* region), mA641\_r (mutations introduced in the *GTTTGTGA* region), and A691 (used as the negative control that contained a 50-bp sequence upstream of A641). While MYB30 showed a strong binding activity to A641 (Fig. 4C), it did not show binding activity to the control sequence (A691) or to the mutated binding sequence (mA641). These results strongly indicate that MYB30 specifically binds to the *GTTGTTGTAGGTTTGTGA*-containing A641 region. Moreover, while the binding activity of mA641\_f was almost at the level of the negative control (A691), MYB30 still showed binding activity to the mA641\_r probe. We therefore conclude that MYB30 can specifically bind to the *LTP5* promoter through the *GTTGTTGT* sequence.

To determine where these genes are expressed in the root, we made transcriptional fusions of *LTPG1* (*pLTPG1::GFP*), *LTPG2* (*pLTPG2::GFP*), *LTP5* (*pLTP5::GFP*), and *PME44* (*pPME44::GFP*) and introduced them into the Col-0 background (Fig. 4D and Fig. S7). *pLTPG1::GFP*, *pLTPG2::GFP*, and *pLTP5::GFP* were up-regulated after 500- $\mu$ M H<sub>2</sub>O<sub>2</sub> treatment. These promoter expression patterns were similar to the MYB30 translational fusion. The cell types in which *pLTPG1*, *pLTPG2*, and *pLTP5* were expressed overlapped with MYB30 expression. However, *pPME44* expression was quite low even after H<sub>2</sub>O<sub>2</sub> treatment. These results strongly indicate that MYB30 directly regulates *LTPG1*, *LTPG2*, and *LTP5* expression in the root tip.

**The MYB30 Gene-Regulatory Network Regulates Root Elongation and Impacts Plant Immunity.** To determine if MYB30 target genes, especially the LTP genes, are involved in regulating root growth upon H<sub>2</sub>O<sub>2</sub> treatment, we obtained T-DNA lines with insertions in the *LTPG1* and *LTPG2* loci [a T-DNA insertion in *LTP5* (SALK\_104674) was reported as a gain-of-function mutant (22)] and crossed these two lines to obtain *ltpg1/ltpg2* double mutants. We first verified that these insertions lead to loss of expression (Fig. S8 A and B) and then tested for root-growth responses to H<sub>2</sub>O<sub>2</sub>. Although no change in root length was observed in the *ltpg1* mutant compared with Col-0 plants, we observed significantly longer roots for the *ltpg2* mutant and for the *ltpg1/ltpg2* double mutants after H<sub>2</sub>O<sub>2</sub> treatment (Fig. S8C). Similar to *myb30-2*, *ltpg2* and *ltpg1/ltpg2* possess a longer elongation zone than Col-0 roots upon H<sub>2</sub>O<sub>2</sub> treatment but similarly sized meristematic zones. Overall, these results demonstrate that LTPG2 is involved in regulating cell elongation in response to H<sub>2</sub>O<sub>2</sub>. As all data suggested that *LTPG2* is directly under MYB30 regulation, we aimed to obtain a *ltpg2/myb30* double mutant to test this hypothesis directly. We were not able to generate the double mutant, most likely due to the physical linkage of these loci. Nevertheless, we were able to test this hypothesis by ectopically overexpressing MYB30 in the *ltpg2* background. There, *MYB30-OX* in *ltpg2* mutants showed significantly less reduction of root length than *MYB30-OX* in *myb30-2* mutants (Fig. S8 D–F). These results suggest that LTPG2 is required for a proportion of the MYB30-dependent regulation of root growth and are consistent with the model that MYB30 directly regulates LTPG2.

Interestingly, MYB30 is known as one of the hyper-response (HR) activators upon pathogen attack (23). Moreover, *ltpg1* mutants have been shown to be more susceptible to infection by a fungal pathogen (24), and LTPG1 and LTPG2 have over-

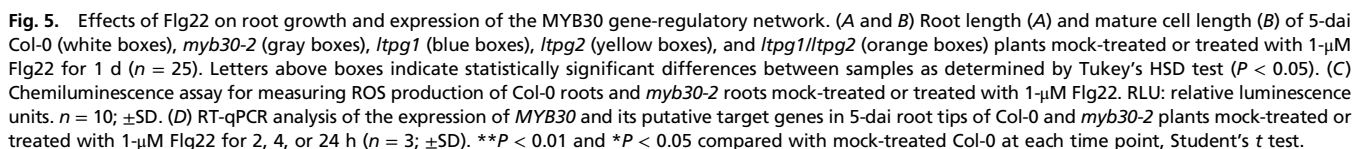
lapping functions in the accumulation of cuticular wax (25). However, these studies were conducted in aerial tissues. Our results led us to hypothesize that, in the root, MYB30 and its target genes could respond to elicitors such as Flg22 produced by plant pathogens. We therefore investigated the effects of Flg22 on root growth of Col-0, *myb30-2*, *ltpg1*, *ltpg2*, and *ltpg1/2* plants by measuring the length of whole roots, the meristematic zone, the elongation zone, and mature cells (Fig. 5 A and B, and Fig. S9). *myb30-2* and *ltpg1/2* roots and mature cell lengths were significantly longer than those of Col-0 plants after treatment with Flg22 for 24 h. However, ROS levels were similarly increased after 150 min of Flg22 treatment in both Col-0 and *myb30-2* plants (Fig. 5C). Thus, MYB30 is sufficient to regulate root length in response to Flg22, but this is due not to altered ROS biosynthesis but most likely to a defect in signaling that is downstream of ROS production.

This prompted us to determine the transcriptional response of MYB30 and its target genes upon Flg22 treatment. MYB30 showed a peak of expression at 2 h after Flg22 treatment and a decrease after 4 h of Flg22 treatment continuing until 24 h, demonstrating that its expression is induced upon Flg22 treatment. Concomitantly with a role of MYB30 as a transcriptional activator, several of its target genes were induced by Flg22 treatment in Col-0 but not in *myb30-2* plants (Fig. 5D). Although LTPG1 expression did not change significantly after Flg22 treatment, LTP5, LTPG2, and PME44 showed significant induction after Flg22 treatment in Col-0 plants. These results indicate that MYB30 and some of its downstream genes control root growth in the presence of a MAMP elicitor.

## Discussion

**ROS-Map Reveals Developmental Zone-Specific Responses to Hydrogen Peroxide.** Using a comprehensive set of microarray experiments, we produced a time-resolved map of transcriptional responses to H<sub>2</sub>O<sub>2</sub> treatment for cells at different developmental stages in the root. These data clearly show that the responses to H<sub>2</sub>O<sub>2</sub> in the meristematic and elongation zones of the root are quite different. Stress-response mechanisms are specifically induced in meristematic cells, presumably protecting cells from oxidative stress. In contrast, no GO categories clearly related to stress response were enriched in the elongation zone even after 6 h of treatment with H<sub>2</sub>O<sub>2</sub>. Instead, genes that relate to the JA and SA pathways, both involved in plant defense signaling, are enriched. Processes relating to the cell wall such as plant-type cell wall organization and polysaccharide biosynthetic process were enriched among genes that were down-regulated in the elongation zone upon H<sub>2</sub>O<sub>2</sub> treatment. These results suggest that H<sub>2</sub>O<sub>2</sub> modifies cell wall composition in the elongation zone. After 6 h of H<sub>2</sub>O<sub>2</sub> treatment, the lipid-transport and lipid-binding categories were found to be enriched among genes that are transcriptionally up-regulated in the elongation zone. Interestingly, this corresponds to the function of the LTP5, LTPG1, and LTPG2, which we identified as being directly regulated by the H<sub>2</sub>O<sub>2</sub>-responsive transcription factor MYB30. These genes execute part of the ROS-response function orchestrated by MYB30. While we focused on LTPG1 and LTPG2, there is evidence from the literature that LTP5 is also involved in root development. A T-DNA insertion line of LTP5 (SALK\_104674) harboring a gain-of-function mutation (22) shows a short-root phenotype (26), and its overexpression affects pollen tube elongation (22). Taken together, these reports strongly suggest that LTP5 is also important for cell elongation.

**Lipid Transfer and Cell Elongation.** While we found genetic evidence for the involvement of LTP5, LTPG1, and LTPG2 in root elongation, the question arises as to how their molecular function relates to this cellular process. This might be related to their function in the cuticle, as the *ltpg1*-, *ltpg2*-, and *ltpg1/ltpg2*-mutant plants have reduced wax and VLCFAs, a primary constituent of the cuticular wax, on the surface of stems and leaves (25, 27). This is in line with a known function of the regulator MYB30, which has



shows a reduction but not depletion of VLCFA levels, exhibits strong growth defects throughout the entire plant body (37). Nevertheless, our genetic approach using *ltpg2* mutants, in which the transport and/or accumulation of cuticular waxes is impaired (25), supports the notion that VLCFA transport to cell surfaces is involved in root cell elongation or its regulation.

In summary, we have generated a transcriptomic dataset, the ROS-map, in which we found a gene-regulatory network that modulates plant growth partly through VLCFA transport. Importantly, this network also impinges on the response to defense



cues. Therefore, we have uncovered a network integrating different aspects of H<sub>2</sub>O<sub>2</sub> signaling.

## Materials and Methods

**Plant Materials and Growth Conditions.** *A. thaliana* Col-0 was used as the wild type. The T-DNA insertion lines *myb30-1* (SALK\_122884), *myb30-2* (SALK\_027644C), *ltpg1* (CS878046), and *ltpg2* (SALK\_016947) were obtained from the SALK collection and the seed stock center of the Arabidopsis Biological Resource Center (ABRC). These mutants were genotyped using left-border primers on the T-DNA (LB), right-side primers on the genome (RP), and left-side primers on the genome (LP) (Table S1). The *ltpg1/ltpg2* double mutants were obtained by crossing *ltpg1* and *ltpg2* homozygous mutants.

All seeds were sterilized by treatment with 1% bleach and 0.05% Triton X-100 for 5 min and then three washings with sterilized water. Seeds were germinated on MS medium (Wako) supplemented with 1% sucrose and 1% agarose after 2 d at 4 °C. Plants were grown vertically in a growth chamber (Panasonic) at 22 °C under 16-h light/8-h dark conditions.

For H<sub>2</sub>O<sub>2</sub>, estradiol, and Flg22 treatments, 5 d after imbibition (dai) seedlings were transferred onto MS medium containing 1-mM H<sub>2</sub>O<sub>2</sub> (for microarray analysis), 500-μM H<sub>2</sub>O<sub>2</sub>, 5-μM estradiol (Wako), and 1-μM Flg22 (EZBiolab), respectively.

**Microarray Experiments.** Total RNA was isolated from the meristematic and elongation zones of roots of 30 Col-0 plants treated with either control medium or medium containing 1 mM H<sub>2</sub>O<sub>2</sub> for 0, 1, 3, or 6 h. Two biological replicates were conducted for each experiment. Fragmented cRNA probes were synthesized using the two-cycle amplification kit (Affymetrix). Samples were submitted to Expression Analysis, Inc. for hybridization to the *Arabidopsis* whole-genome ATH1 Affymetrix GeneChip (Affymetrix).

**Microarray Data Analysis.** Microarray datasets were analyzed by using R packages. For background correction, normalization and expression estimates were computed using gcRMA ([www.bioconductor.org](http://www.bioconductor.org)) (39). For global analysis of the transcriptome responses, the false-discovery rates (FDRs) were calculated by the Significance Analysis of Microarray (SAM) algorithm (40). Differentially expressed genes were identified based on fold change (FC) in expression and a significant *P* value (FC > 2 and *P* value < 0.05) compared with control treatment at each time point. Enriched GO categories were analyzed by ChipEnrich software (41). The TMeV program ([www.tigr.org](http://www.tigr.org)) was used for visualizing of the heat map for enriched GO categories and FCs of expression of transcription. All microarray data were submitted to the National Center for Biotechnology Information Gene Expression Omnibus database under accession number GSE85015.

**Plasmid Construction and Plant Transformation.** Plasmids were constructed using Gateway cloning technology (Thermo Fisher Scientific). Genomic DNA from Col-0 plants was used as the template for amplification of the regions 3,045 bp upstream of *MYB30* gene, 2,105 bp upstream of *LTP5* gene, 2,610 bp upstream of *LTPG1*, 3,000 bp upstream of *LTPG2*, and 1,808 bp upstream of *PME44* gene for the transcriptional fusions. dA overhangs to the 5' end were added to this PCR amplicon by the Takara Taq polymerase (Takara). It was then cloned into pENTR5-TOPO (Thermo Fisher Scientific). YFP was amplified by a primer set, which contained an attB1 site in front of YFP start codon as the forward primer and an Aor51H1-BamHI site before attB2 as the reverse primer. attB1-YFP-Aor51H1-BamHI-attB2 fragments were cloned into pDonr201 by BP-Clonase (Thermo Fisher Scientific). The *MYB30* cDNA region was amplified by a forward primer and reverse primer that contained a BamHI site just before the *MYB30* termination codon. Then *MYB30*-BamHI fragments were cloned into the Aor51H1 and BamHI sites of YFP-Aor51H1-BamHI-pDonr201 plasmids. For the *35S::YFP-MYB30* and *pXVE::YFP-MYB30* constructs, YFP-MYB30 containing pDonr201 was cloned into pGWB502Δ (42) and pMDC7 (18), respectively, by using LR-Clonase II (Thermo Fisher Scientific). For the *pMYB30::GFP*, *pLTP5::GFP*, *pLTPG1::GFP*, *pLTPG2::GFP*, and *pPME44::GFP*, *MYB30*, *LTP5*, *LTPG1*, *LTPG2*, and *PME44* promoter regions containing pENTR5-TOPOs were cloned into R4L1pGWB550 (43) by using LR-Clonase II. For the *pMYB30::YFP-MYB30* construct, the *MYB30* promoter region containing pENTR5-TOPO and YFP-MYB30 containing pDonr201 were cloned into R4pGWB501 (44) by using LR-Clonase II. The resulting plasmids (*pMYB30::GFP*, *pLTP5::GFP*, *pLTPG1::GFP*, *pLTPG2::GFP*, *pPME44::GFP*, *pMYB30::YFP-MYB30*, *35S::YFP-MYB30*, and *pXVE::YFP-MYB30*) were transferred into *Agrobacterium* and were used to transform into Col-0, *myb30-1*, *myb30-2*, and *ltpg2*. The primers used in these studies are listed in Table S1.

**Real-Time RT-qPCR.** RNA was isolated from whole roots of 5-dai plants treated with control medium or 500-μM H<sub>2</sub>O<sub>2</sub> using the RNeasy plant kit (QIAGEN). For isolation of RNA from the root tip, root tips of 6-dai plants that contained meristematic and elongation zones were microdissected (6). The RNeasy micro kit (QIAGEN) was then used for RNA isolation. First-strand cDNA was synthesized using the ReverTra Ace qPCR RT Master Mix with gDNA Remover (TOYOBO). RT-qPCR was performed using THUNDERBIRD SYBR qPCR Mix (TOYOBO) on an Illumina Eco real-time PCR system (Illumina). The primers used in this study are listed in Table S1. RT-qPCR efficiency and the cycle threshold (CT) value were determined by using the standard curves for each primer set. Efficiency-corrected transcript values of three biological replicates for all samples were used for determining the relative expression values. The level of each value was normalized against the level of *PDF2* (45).

**ChIP-qPCR Experiment.** Over 1,200 plants of the *p35S::YFP-MYB30/myb30-1* T<sub>2</sub> line and Col-0 plants were grown on MS medium for 6 d. Whole roots were fixed, and ChIP was performed by the protocol described in ref. 46. Eluted solutions were used as templates for qPCR. Three biological replicates of all samples were used for determining the enrichment. Col-0 genomic DNA was used as the template for making the standard curves for each primer set. The enrichments were calculated by using the qPCR values from each input fraction. The primers used in this study are listed in Table S1.

**Synthesis of Recombinant Proteins.** Protein synthesis was performed with the IN VITRO Transcription/Translation Reagents kit following the manufacturer's instructions (BioSieg). For in vitro transcription, the DNA coding sequence of the FLAG tag (DYKDDDDK) was attached to the coding sequence of *MYB30* by the KOD-Plus-Neo DNA polymerase (TOYOBO). Around 30 μg of RNA was transcribed by T7 RNA polymerase from the PCR product. The transcribed RNA was mixed with 10 μL of a wheat germ extract and 10 μL of amino acid mixture (BioSieg) at 16 °C for 10 h. The synthesized *MYB30* protein was confirmed by immunoblotting with an antibody against FLAG (Wako).

**In Vitro Protein DNA-Binding Assay (AlphaScreen System).** In vitro protein-DNA interactions were evaluated by the AlphaScreen system (PerkinElmer, Inc.) according to the manufacturer's instructions. DNA probes were obtained by annealing a 5'-biotinylated 50-base ssDNA (Eurofins) to complementary unmodified ssDNAs (Eurofins) (see Table S1 for the sequences). Two microliters of four-times diluted FLAG-tagged *MYB30* and 1 μL of 625-nM DNA double-strand probes were incubated with 2.5 μL of 10× control buffer [FLAG (M2) Detection Kit; PerkinElmer Inc.], 2.5 μL of 0.1% (wt/vol) Tween 20, 2.5 μL of 1% (wt/vol) BSA, 1 μL of 1 ng/μL of sAdT (PerkinElmer, Inc.), and 5.5 μL of ultrapure water at room temperature for 1 h. The reaction samples were mixed with 4 μL of 40-fold diluted Acceptor beads (PerkinElmer) and then were incubated for 1 h, followed by reaction with 4 μL of 40-fold diluted Donor beads for 1 h in the dark. After the excitation at 680 nm, the emission wavelengths between 520 and 620 nm were measured as AlphaScreen unit by using an EnSpire Alpha 2390 Multilabel Reader (PerkinElmer Inc.).

**RNA-Seq Experiments.** The cDNA libraries were generated from 100 ng of total RNA samples by a TruSeq RNA sample preparation kit (Illumina) as described previously (47), and the amount of cDNA was determined by Phix Control (Illumina). Both ends of the cDNA libraries were sequenced for 60 cycles using a paired-end module. Two biological replicates were conducted for each experiment.

**RNA-Seq Data Analysis.** The short read results from sequencing were mapped onto the *Arabidopsis* genome (TAIR10: [www.arabidopsis.org](http://www.arabidopsis.org)) by Bowtie software (48). Then these datasets were normalized, and an FDR and an FC were calculated using the edgeR package for R (49). We used an FC > 2 and an FDR of *q* < 0.01 as the cut-off values to determine differentially expressed genes among Col-0, *myb30-2*, and *35S::YFP-MYB30/myb30-1* T<sub>2</sub> plants. The data were deposited in the DNA Data Bank of Japan (DDBJ) Sequence Read Archive (DRA) (<http://www.ddbj.nig.ac.jp/index-e.html>) with the accession number DRA005125.

**Phenotypic and Microscopic Analyses.** For measuring the whole root length, roots were scanned using a GT-7400U flatbed scanner (Epson) while growing on plates. The root length was measured using ImageJ software (NIH) on the scanned images. Laser-scanning confocal microscopy was performed using a Leica SP8 system (Leica) on propidium iodide-stained roots. For time-lapse imaging, a Lab-Tek Chambered Coverglass with cover (Thermo Fisher Scientific)

was used. At 5 dai, seedlings on MS or treatment medium were placed on the coverglass, which was located at the bottom of the chamber. Then the chamber containing the plants was imaged with a DMI6000B-AFC fluorescence microscope (Leica) and an SP8 confocal microscope (Leica). Time-lapse images were taken by LAS X software (Leica) every 20 min for 20 h. Assembly and measurement of relative fluorescent intensity were also done with LAS X software. The root-elongation rate was measured by ImageJ software on time series consisting of images taken every 20 min.

**ROS Measurements.** ROS production was measured using L-012-mediated chemiluminescence. Six-day-old seedling roots were cut into ~13-mm lengths

from root tip and were dipped in 96-well plates containing 300  $\mu$ L sterile water overnight. Then the water was replaced with 100- $\mu$ M L-012, with/without 100-nM Flg22. Luminescence was measured every 3 min for 8 h using a Mithras<sup>2</sup> LB 943 Multimode Reader (Berthold Technologies).

**ACKNOWLEDGMENTS.** We thank Dr. S. Brady, Dr. R. Sozzani, and Dr. P. N. Benfey for comments on the manuscript and the ABRC for sending seeds. This work was supported by Japan Science and Technology Agency Precursory Research for Embryonic Science and Technology Grant 20115 and Ministry of Education, Culture, Sports, Science, and Technology Grant-in-Aid for Scientific Research on Innovative Areas Grant 26113508 (to H.T.).

- Vanstraelen M, Benková E (2012) Hormonal interactions in the regulation of plant development. *Annu Rev Cell Dev Biol* 28:463–487.
- Tsukagoshi H (2016) Control of root growth and development by reactive oxygen species. *Curr Opin Plant Biol* 29:57–63.
- Yu Q, et al. (2016) A P-loop NTPase regulates quiescent center cell division and distal stem cell identity through the regulation of ROS homeostasis in Arabidopsis root. *PLoS Genet* 12:e1006175.
- Kärkönen A, Kuchitsu K (2015) Reactive oxygen species in cell wall metabolism and development in plants. *Phytochemistry* 112:22–32.
- Lamb C, Dixon RA (1997) The oxidative burst in plant disease resistance. *Annu Rev Plant Physiol Plant Mol Biol* 48:251–275.
- Tsukagoshi H, Busch W, Benfey PN (2010) Transcriptional regulation of ROS controls transition from proliferation to differentiation in the root. *Cell* 143:606–616.
- Tsukagoshi H (2012) Defective root growth triggered by oxidative stress is controlled through the expression of cell cycle-related genes. *Plant Sci* 197:30–39.
- Burke JJ, Gamble PE, Hatfield JL, Quisenberry JE (1985) Plant morphological and biochemical responses to field water deficits: I. Responses of glutathione reductase activity and paraquat sensitivity. *Plant Physiol* 79:415–419.
- Apel K, Hirt H (2004) Reactive oxygen species: Metabolism, oxidative stress, and signal transduction. *Annu Rev Plant Biol* 55:373–399.
- Dinneny JR, et al. (2008) Cell identity mediates the response of Arabidopsis roots to abiotic stress. *Science* 320:942–945.
- Peleg-Grossman S, Melamed-Book N, Levine A (2012) ROS production during symbiotic infection suppresses pathogenesis-related gene expression. *Plant Signal Behav* 7:409–415.
- Denness L, et al. (2011) Cell wall damage-induced lignin biosynthesis is regulated by a reactive oxygen species- and jasmonic acid-dependent process in Arabidopsis. *Plant Physiol* 156:1364–1374.
- Albert M (2013) Peptides as triggers of plant defence. *J Exp Bot* 64:5269–5279.
- Gómez-Gómez L, Felix G, Boller T (1999) A single locus determines sensitivity to bacterial flagellin in Arabidopsis thaliana. *Plant J* 18:277–284.
- Rizhsky L, Davletova S, Liang H, Mittler R (2004) The zinc finger protein Zat12 is required for cytosolic ascorbate peroxidase 1 expression during oxidative stress in Arabidopsis. *J Biol Chem* 279:11736–11743.
- Mittler R, et al. (2006) Gain- and loss-of-function mutations in Zat10 enhance the tolerance of plants to abiotic stress. *FEBS Lett* 580:6537–6542.
- Sakuma Y, et al. (2006) Functional analysis of an Arabidopsis transcription factor, DREB2A, involved in drought-responsive gene expression. *Plant Cell* 18:1292–1309.
- Moore I, Samalova M, Kurup S (2006) Transactivated and chemically inducible gene expression in plants. *Plant J* 45:651–683.
- Aoki Y, Okamura Y, Tadaka S, Kinoshita K, Obayashi T (2016) ATTED-II in 2016: A plant coexpression database towards lineage-specific coexpression. *Plant Cell Physiol* 57:e5.
- Brady SM, et al. (2007) A high-resolution root spatiotemporal map reveals dominant expression patterns. *Science* 318:801–806.
- Li L, et al. (2009) Arabidopsis MYB30 is a direct target of BES1 and cooperates with BES1 to regulate brassinosteroid-induced gene expression. *Plant J* 58:275–286.
- Chae K, Kieslich CA, Morikis D, Kim SC, Lord EM (2009) A gain-of-function mutation of Arabidopsis lipid transfer protein 5 disturbs pollen tube tip growth and fertilization. *Plant Cell* 21:3902–3914.
- Raffaele S, et al. (2008) A MYB transcription factor regulates very-long-chain fatty acid biosynthesis for activation of the hypersensitive cell death response in Arabidopsis. *Plant Cell* 20:752–767.
- Lee SB, et al. (2009) Disruption of glycosylphosphatidylinositol-anchored lipid transfer protein gene altered cuticular lipid composition, increased plastoglobules, and enhanced susceptibility to infection by the fungal pathogen *Alternaria brassicicola*. *Plant Physiol* 150:42–54.
- Kim H, et al. (2012) Characterization of glycosylphosphatidylinositol-anchored lipid transfer protein 2 (LTPG2) and overlapping function between LTPG/LTPG1 and LTPG2 in cuticular wax export or accumulation in Arabidopsis thaliana. *Plant Cell Physiol* 53:1391–1403.
- Chae K, et al. (2010) A multifaceted study of stigma/style cysteine-rich adhesin (SCA)-like Arabidopsis lipid transfer proteins (LTPs) suggests diversified roles for these LTPs in plant growth and reproduction. *J Exp Bot* 61:4277–4290.
- Debono A, et al. (2009) Arabidopsis LTPG is a glycosylphosphatidylinositol-anchored lipid transfer protein required for export of lipids to the plant surface. *Plant Cell* 21:1230–1238.
- Narukawa H, Yokoyama R, Komaki S, Sugimoto K, Nishitani K (2015) Stimulation of cell elongation by tetraploidy in hypocotyls of dark-grown Arabidopsis seedlings. *PLoS One* 10:e0134547.
- Xia Y, Nikolau BJ, Schnable PS (1996) Cloning and characterization of CER2, an Arabidopsis gene that affects cuticular wax accumulation. *Plant Cell* 8:1291–1304.
- Li Y, et al. (2007) Identification of acyltransferases required for cutin biosynthesis and production of cutin with suberin-like monomers. *Proc Natl Acad Sci USA* 104:18339–18344.
- Andersen TG, Barberon M, Geldner N (2015) Suberization—The second life of an endodermal cell. *Curr Opin Plant Biol* 28:9–15.
- Schreiber L, Franke R, Hartmann K (2005) Wax and suberin development of native and wound periderm of potato (*Solanum tuberosum* L.) and its relation to peridermal transpiration. *Planta* 220:520–530.
- Razem FA, Bernards MA (2003) Reactive oxygen species production in association with suberization: Evidence for an NADPH-dependent oxidase. *J Exp Bot* 54:935–941.
- Kosma DK, et al. (2014) AtMYB41 activates ectopic suberin synthesis and assembly in multiple plant species and cell types. *Plant J* 80:216–229.
- Lee SB, Suh MC (2015) Cuticular wax biosynthesis is up-regulated by the MYB94 transcription factor in Arabidopsis. *Plant Cell Physiol* 56:48–60.
- Beaudoin F, et al. (2009) Functional characterization of the Arabidopsis beta-ketoacyl-coenzyme A reductase candidates of the fatty acid elongase. *Plant Physiol* 150:1174–1191.
- Bach L, et al. (2008) The very-long-chain hydroxy fatty acyl-CoA dehydratase PASTICINO2 is essential and limiting for plant development. *Proc Natl Acad Sci USA* 105:14727–14731.
- Eichmann R, Schäfer P (2015) Growth versus immunity—A redirection of the cell cycle? *Curr Opin Plant Biol* 26:106–112.
- Gentleman RC, et al. (2004) Bioconductor: Open software development for computational biology and bioinformatics. *Genome Biol* 5:R80.
- Tusher VG, Tibshirani R, Chu G (2001) Significance analysis of microarrays applied to the ionizing radiation response. *Proc Natl Acad Sci USA* 98:5116–5121.
- Orlando DA, Brady SM, Koch JD, Dinneny JR, Benfey PN (2009) Manipulating large-scale Arabidopsis microarray expression data: Identifying dominant expression patterns and biological process enrichment. *Methods Mol Biol* 553:57–77.
- Nakagawa T, et al. (2007) Improved gateway binary vectors: High-performance vectors for creation of fusion constructs in transgenic analysis of plants. *Biosci Biotechnol Biochem* 71:2095–2100.
- Nakamura S, et al. (2009) Development of gateway binary vectors, R4L1pGWBs, for promoter analysis in higher plants. *Biosci Biotechnol Biochem* 73:2556–2559.
- Nakagawa T, et al. (2008) Development of R4 gateway binary vectors (R4pGWB) enabling high-throughput promoter swapping for plant research. *Biosci Biotechnol Biochem* 72:624–629.
- Czechowski T, Stitt M, Altmann T, Udvardi MK, Scheible WR (2005) Genome-wide identification and testing of superior reference genes for transcript normalization in Arabidopsis. *Plant Physiol* 139:5–17.
- Kamiya T, et al. (2015) The MYB36 transcription factor orchestrates Casparian strip formation. *Proc Natl Acad Sci USA* 112:10533–10538.
- Tsukagoshi H, et al. (2015) RNA-seq analysis of the response of the halophyte, *Mesembryanthemum crystallinum* (ice plant) to high salinity. *PLoS One* 10:e0118339.
- Langmead B, Trapnell C, Pop M, Salzberg SL (2009) Ultrafast and memory-efficient alignment of short DNA sequences to the human genome. *Genome Biol* 10:R25.
- Robinson MD, McCarthy DJ, Smyth GK (2010) edgeR: A bioconductor package for differential expression analysis of digital gene expression data. *Bioinformatics* 26:139–140.